Measurements of Neutrons from Photonuclear Reactions Using Laser Compton Scattering Gamma Rays*)

Shuji MIYAMOTO, Akinori TAKEMOTO, Masashi YAMAGUCHI, Kento SUGITA, Satoshi HASHIMOTO and Sho AMANO

Laboratory of Advanced Science and Technology for Industry, University of Hyogo, Hyogo 678-1205, Japan

(Received 10 August 2017 / Accepted 2 December 2017)

The laser Compton scattering gamma ray beamline at the synchrotron light facility NewSUBARU supplies a quasi-monochromatic, polarized, high-energy photon beam. A gamma ray flux of more than 10^7 photons/s is generated at a photon energy range of 1 - 73 MeV. Emission distributions of the fast neutrons generated from different target materials were measured as a function of the polarization angle of the linear polarized gamma-ray beam using a time-of-flight method with fast plastic scintillators. The neutron distributions were consistent with a previous theoretical result. The relatively slow neutrons were measured via an activation method. The result demonstrated the small anisotropy of the slow neutron emission.

Keywords: neutron, gamma ray, laser Compton scattering, photonuclear reaction, electron storage ring, synchrotron light, time-of-flight, activation

DOI: 10.1585/pfr.13.2404066

1. Introduction

The NewSUBARU Synchrotron Light Facility [1] consists of a electron storage ring of GeV-energy electron and nine beamlines that use the synchrotron radiation. One of the beamlines (BL01) was constructed as a laser Compton scattering gamma-ray source. Here, it is possible to ghenerate gamma-ray energies of 1 - 73 MeV with a flux of 10^7 gamma photons/sec [2–6]. This gamma-ray beam source is generated via collisions between the laser beam and the relativistic electron beam in the electron storage ring. In the case of head-on collisions, the scattered photon energy E_γ is estimated from the relativistic Doppler shift of the photon energy as

$$E_\gamma(\theta) = \frac{4E_L\gamma^2}{1+\gamma^2\theta^2+\dfrac{4E_L\gamma}{mc^2}}, \quad (1)$$

where $\gamma = E_e/mc^2$ is Lorenz factor of the electron, E_e is the electron kinetic energy, mc^2 is the electron rest energy, E_L is the laser photon energy, $4E_L\gamma/mc^2$ is the recoil effect of the scattered photon to the electron, and θ is the angle of the scattered photon relative to the electron beam axis. A typical gamma ray photon energy is calculated to be 16.9 MeV in the case where an electron energy of 982 MeV and an Nd:YVO_4 laser (with a wavelength of 1.064 μm) is used. The gamma ray photon energy can be changed by changing the electron energy or the laser photon energy. One additional excellent feature of this gamma ray source is its directed beam source with a small divergence angle. The above Eq. (1) shows that the scattered photon energy depends on the angle of the scattered photon. Therefore, a quasi-monochromatic gamma ray beam can be obtained by inserting a collimator to restrict the angle of the scattered photon. For example, when we use a collimator with a diameter of 3 mm at a distance of 17 m from the scattering point, the energy spread of the gamma ray beam is approximately 3% for an electron energy of 1-GeV.

Over the past few years, this gamma ray beam source has been used for research in various fields such as nuclear transmutation for nuclear waste disposal [7–9], useful radio-isotope generation [10, 11], nuclear physics studies [12–16], nuclear astrophysics studies [17], positron generation and application to non-destructive inspections of materials [18, 19], and detector tests via a high-energy polarized photon beam [20].

In this paper, we report photo-neutron emission distribution measurements using fast scintillation detectors and dysprosium (Dy) activation detectors. In a previous paper [15], we discussed the fact that the emission distribution of photo-neutrons as a function of gamma ray polarization includes information concerning the nucleus structure of the gamma-ray target. Here we measure photonuclear reactions using various targets with linearly polarized gamma-ray beams. Nearly all nuclei have large photonuclear reaction cross sections at the photon energies of several tens of MeV due to the Giant Dipole Resonance (GDR). For example, the gold nucleus has a more than 500 mb peak cross section at a gamma-ray energy of 13.5 MeV with a resonance width of approximately 5 MeV. In this photon energy region, the primary absorption mechanisms of the

author's e-mail: miyamoto@lasti.u-hyogo.ac.jp

*) This article is based on the presentation at the Conference on Laser Energy Science / Laser and Accelerator Neutron Sources and Applications 2017.

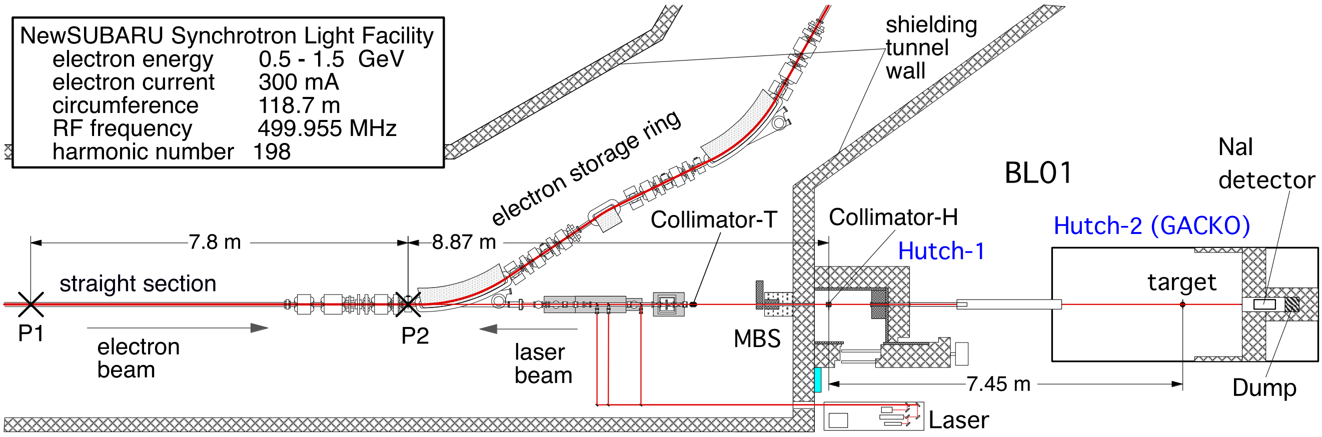

Fig. 1 The laser Compton gamma ray beamline (BL01) in the NewSUBARU synchrotron light facility. One sixth part of the electron storage ring is shown. The storage electron bunches rotate in a counter-clockwise manner. Laser beams are injected from the outside of the shielding tunnel in which the storage ring is installed. The laser photons collide with electrons at the collision points P1 or P2 and are scattered back to the irradiation hutches 1 and 2.

gamma ray are pair creation and Compton scattering. Both mechanisms generate prompt gamma rays in the target and are detected by the scintillation neutron detectors. To distinguish the neutron from such gamma-ray noise, the time-of-flight method was used for the fast neutron measurements.

2. Experimental Setup

Figure 1 shows the experimental layout of the BL01 gamma ray beamline at NewSUBARU. The electron storage ring consists of six cells of a double bend achromat lattice (DBA lattice) with inverse bend magnets [1]. The laser Compton scattering gamma ray beamline BL01 is located downstream of the straight section. The laser beam is injected from outside the shielding tunnel in which the electron storage ring is installed. Two collision points, P1 and P2, exist. Collision point P2 is used for the long wavelength lasers. Short wavelength lasers (Nd lasers:1.064 µm and 0.532 µm and an Er laser:1.55 µm) use the collision point P1. The length from P1 to the target position in the gamma ray irradiation hutch is 24.1 m. A typical gamma ray beam size is 2 cm in diameter. Figure 2 (a) shows a gamma ray beam image taken by an imaging plate (Fuji Film BAS-SR2025). The pixel size of the imaging plate was 0.05 mm and the image size is 55 mm × 55 mm. This image was taken several years ago with a gamma ray peak energy of 1.7 MeV. A vertically polarized CO_2 laser was used for the Compton scattering of the 1-GeV electrons. In this figure, a circle with a diameter 6 mm is added as a reference of the collimator size. The gamma-ray band width with this collimator is approximately 30%. The image was extended horizontally due to the vertically polarized laser scattering. The photon scattering is a dipole radiation from the electron vibrated by the electric field of the incident photon at the electron rest frame. The emission distribution has a $\sin^2\theta$ shape. θ is the angle from the dipole vibration axis. This emission distribution was transformed to the laboratory frame resulting in an elliptical shape with its long axis perpendicular to the photon polarization direction, as shown in Fig. 2.

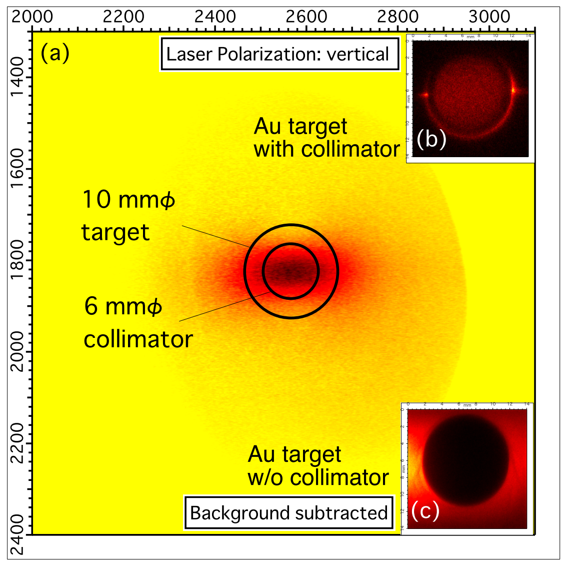

Fig. 2 (a) Polarized gamma ray beam image taken by an imaging plate with a 1.7-MeV gamma ray. (b) and (c) The target alignment and target irradiation monitor images taken by an Si-pixel monitor with a 16.7-MeV gamma ray.

The insets of Fig. 2, Figs. 2 (b) and 2 (c) are the target alignment and target irradiation monitor images taken by a 14 mm × 14 mm Si-pixel monitor (Advacam MiniPix, Si:500 µm, 256 × 256 pixels). The upper image shows a transmitted gamma ray through a 10-mm-diameter 40-mm-long gold target irradiated by a 16.9-MeV gamma-ray beam with a 6 mm collimator. The collimated gamma beam and gold rod target were well aligned. In this case, an Nd:YVO_4 laser was used.

The setup of the time-of-flight (TOF) neutron measurements was the same as the previous experiment reported in Ref. [5] except that the irradiation hutch was used. Previous measurements were performed in hutch-1 instead of hutch-2, which was used in the present experiments. Single bunch electrons (E_e = 982 MeV) were used. In this mode, only one electron bunch with a 60-ps pulse width (FWHM) circulates in the NewSUBARU electron storage ring with a 2.5 MHz revolution frequency and the storage current is limited to 20 mA. The laser (Nd laser, λ = 1064 nm) was also operated with a 60-ns pulse width pulse mode and a 25 kHz repetition rate with an average power of 15 W. The timing between the electrons and the laser bunch was adjusted for a collision at collision point P1. The gamma-ray arriving time on the target was precisely synchronized with the electron bunch of 60 ps, even thouth the laser pulse width was 60 ns. Then, a divided synthesizer frequency of 25 kHz was used as a trigger of the laser and the stop signal of the TAC (time-amplitude-converter) module. The neutron detector signal was used as a start trigger of the TAC module. The neutron detector consists of a fast plastic scintillator and a photo multiplier tube (time response of approximately 2 ns). The irradiated target was 10-mm-diameter and 40-mm-long rod. After aligning the target at the center of the gamma-ray beam, the collimator was not used. The flight path of the neutrons (from the target to the neutron detector) was 1 m. The data accumulation time was typically 2 h. We measured the neutron emission intensity distribution as a function of the gamma-ray polarization angle. Neutron generating target of ^{197}Au, ^{107,109}Ag and ^{89}Y were tested. All targets used had natural isotopic abundance nuclei.

Low-energy neutron measurements were made using an activation method. Figure 3 shows a layout of the Dy activation foils and the neutron-generating target. The gamma-ray beam irradiates the central gold target (10 mmϕ × 40 mm), and a photo-neutron is emitted in the 4π direction. The neutrons are thermalized in the moderator polyethylene and are absorbed by four Dy activation targets (25 mm × 25 mm × 0.25 mm) located in the moderator. Natural Dy foils are used. The natural abundance of ^{164}Dy is 28%. The neutron absorption and decay reaction of Dy is ^{164}Dy(n)^{165}Dy(β^-)^{165}Ho. The half-life of ^{165}Dy is 2.33 h. Therefore, an irradiation time of approximately 4 h is suitable. After irradiation, activated Dy foils are sandwiched with imaging plates to transcribe the decay β^- and γ for approximately 10 h.

3. Results

The emission distribution of neutron from ^{197}Au(γ, n)^{196}Au reaction measured via the TOF method has shown relatively large anisotropy in previous experiments [21]. In the present experiments, we used the Au target as a standard target to compare to previous results. Our result is in good agreement with previous results. Therefore, we consider the new measurement system as being consistent with the previous one. The neutron emission distribution as a function of the azimuthal angle refers to the polarization direction of the gamma ray following $I_n = a + b \cdot \cos(2\phi)$. This function is Agodi's prediction [22]. Figure 4 shows the neutron emission distribution from the Y and Ag targets. The results of the two new targets show similar distribution dependence. However, the target mass number dependence of the distribution anisotropy shows a different trend from before. Previous experiments showed that the strength of the neutron emission anisotropy was roughly proportional to the mass number of the nucleus [5] (Fig. 5). The new date of Y and Ag data are added as circles in Fig. 5. The results show that the anisotropy depends on other parameters of the nucleus instead of, or not only on, the atomic mass number.

Figure 6 shows data of a low-energy neutron measurement via an activation method. The four dark square images are the transcribed images from the four Dy activation foils. Vertically integrated intensity line profiles

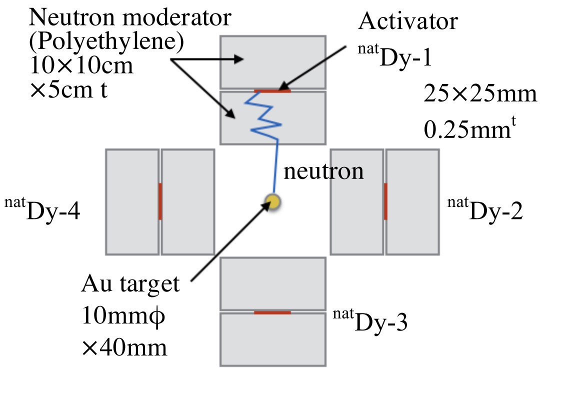

Fig. 3 The layout of the four Dy activation foils and the neutron-emitting Au target. The gamma-ray beam irradiates the target vertically to the page, from back to front.

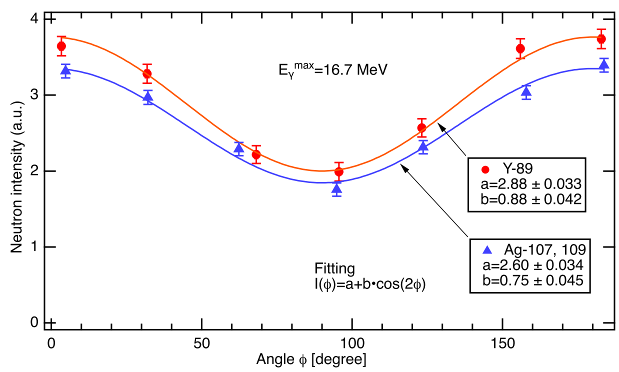

Fig. 4 The neutron emission distribution from Y and Ag targets. The fitting curves have $a + b \cdot \cos(2\phi)$ distribution.

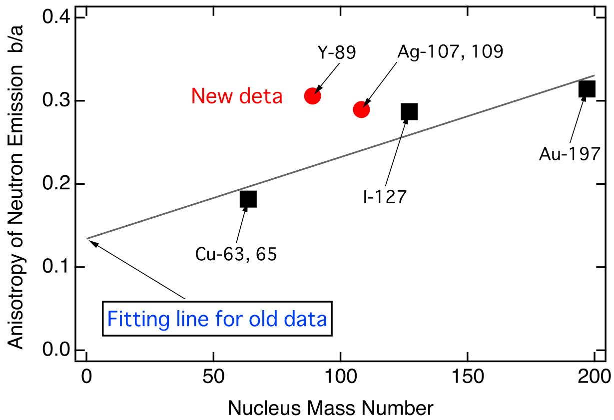

Fig. 5 Neutron emission anisotropy dependence on the nucleus mass number. Anisotropy is indicated by the value of b/a with a neutron emission distribution of $a + b \cdot \cos(2\phi)$.

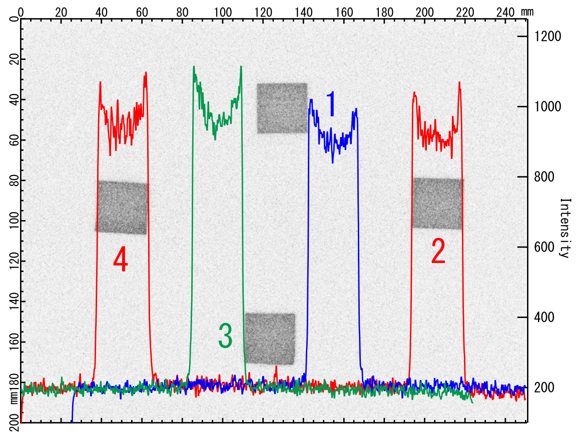

Fig. 6 Transcribed images of dysprosium activation on an imaging plate. Four dark squares are the Dys. Vertically integrated intensity line profiles are added. The two end profiles and the central two profiles are data from horizontally and vertically located samples, respectively.

are added. The two end profiles are data from a horizontally located sample and the central two profiles are from a vertically positioned sample. The right vertical axis indicates the intensity for the integrated line profile. All images have an intensity of approximately 800 - 1000. These low-energy data show no or little anisotropy in the neutron emission. The edge of each line profile have high intensity peaks. These profiles indicate the thermalized neutrons in the polyethylene moderator accumulated by the Dy foils. This means that an optimized design of the moderator is required to measure the neutron emission anisotropy due to the reduction of the angular sensitivity by the crosstalk of neutrons.

Acknowledgments

We would like to thank Takehito Hayakawa (QST), Yasuhiro Asano (RIKEN) and Toshiro Itoga (JASRI) for valuable discussions. This work was supported by “Establishment of basic technologies for compact neutron sources and industrial applications/Development of laser-driven neutron source and application to fast radiography” (AS2721002c), A-STEP, JST.

[1] A. Ando *et al.*, J. Synchrotron Radiat. **5**, 342 (1998).
[2] S. Miyamoto *et al.*, Radiat. Meas. **41**, S179 (2007).
[3] S. Amano *et al.*, Nucl. Instrum. Methods Phys. Res. A **602**, Issue 2, 337 (2009).
[4] K. Horikawa, S. Miyamoto, S. Amano and T. Mochizuki, Nucl. Instrum. Methods Phys. Res. A **618**, 209 (2010).
[5] S. Miyamoto, Rev. Laser Eng. **41**, 917 (2013).
[6] H. Utsunomiya, S. Hashimoto and S. Miyamoto, Nucl. Phys. News **25**, Issue 3, 25 (2015).
[7] D. Li *et al.*, J. Nucl. Sci. Technol. **46**, 831 (2009).
[8] K. Horikawa *et al.*, Rev. Laser Eng. **39**, 445 (2011).
[9] T. Hayakawa, S. Miyamoto, R. Hajima, T. Shizuma, S. Amano, S. Hashimoto and T. Misawa, J. Nucl. Sci. Technol. **53**, 2064 (2016).
[10] H. Ejiri, T. Shima, S. Miyamoto, K. Horikawa, Y. Kitagawa, Y. Asano, S. Date’ and Y. Ohashi, J. Phys. Soc. Jpn. **80**, 094202 (2011).
[11] M. Fujiwara, K. Nakai, N. Takahashi, T. Hayakawa, T. Shizuma, S. Miyamoto, G.T. Fan, A. Takemoto, M. Yamaguchi and M. Nishimura, Phys. Part. Nuclei **48**, 124 (2017).
[12] K. Horikawa, S. Miyamoto, T. Mochizuki, S. Amano, D. Li, K. Imasaki, Y. Izawa, K. Ogata, S. Chiba and T. Hayakawa, Phys. Lett. B **737**, 109 (2014).
[13] D.M. Filipescu, I. Gheorghe, H. Utsunomiya, S. Goriely, T. Renstrøm, H.-T. Nyhus, O. Tesileanu, T. Glodariu, T. Shima, K. Takahisa, S. Miyamoto, Y.-W. Lui, S. Hilaire, S. Pe’ru, M. Martini and A.J. Koning, Phys. Rev. C **90**, 064616 (2014).
[14] H. Utsunomiya, S. Katayama, I. Gheorghe, S. Imai, H. Yamaguchi, D. Kahl, Y. Sakaguchi, T. Shima, K. Takahisa and S. Miyamoto, Phys. Rev. C **92**, 064323 (2015).
[15] T. Hayakawa, T. Shizuma, S. Miyamoto, S. Amano, A. Takemoto, M. Yamaguchi, K. Horikawa, H. Akimune, K. Ogata and M. Fujiwara, Phys. Rev. C **93**, 004313 (2016).
[16] T. Yamagata, S. Nakayama, H. Akimune and S. Miyamoto, Phys. Rev. C **95**, 044307 (2017).
[17] T. Shima, Y. Nagai, S. Miyamoto, S. Amano, K. Horikawa, T. Mochizuki, H. Utsunomiya and H. Akimune, AIP Conf. Proc. **1235**, 315 (2010).
[18] D. Li, K. Imasaki, S. Miyamoto, K. Horikawa, S. Amano and T. Mochizuki, Appl. Phys. Lett. **94**, 091112 (2009).
[19] F. Hori, Y. Ueno, K. Ishii, T. Ishiyama, A. Iwase, S. Miyamoto and M. Terasawa, J. Phys.: Conf. Series **674**, 012025 (2016).
[20] S. Wang, D. Bernard, S. Amano, S. Hashimoto, S. Miyamoto *et al.*, J. Phys.: Conf. Series **650**, 012016 (2015).
[21] S. Miyamoto and K. Horikawa, Rev. Laser Eng. **36**, 798 (2008).
[22] A. Agodi, Nuovo Cimento **5**(1), 21 (1957).